Simulating seeded vacuum decay in a cold atom system

Thomas P. Billam,[1,*] Ruth Gregory,[2,3,†] Florent Michel,[2,‡] and Ian G. Moss[4,§]

[1]*Joint Quantum Centre (JQC) Durham-Newcastle, School of Mathematics, Statistics and Physics,*
Newcastle University, Newcastle upon Tyne, NE1 7RU, United Kingdom
[2]*Centre for Particle Theory, Durham University, South Road, Durham DH1 3LE, United Kingdom*
[3]*Perimeter Institute, 31 Caroline Street North, Waterloo, Ontario N2L 2Y5, Canada*
[4]*School of Mathematics, Statistics and Physics, Newcastle University,*
Newcastle upon Tyne NE1 7RU, United Kingdom

We propose to test the concept of seeded vacuum decay in cosmology using a Bose-Einstein condensate system. The role of the nucleation seed is played by a vortex within the condensate. We present two complementary theoretical analyses that demonstrate seeded decay is the dominant decay mechanism of the false vacuum. First, we adapt the standard instanton methods to the Gross-Pitaevskii equation. Second, we use the truncated Wigner method to study vacuum decay.

I. INTRODUCTION

First-order phase transitions form an important class of physical phenomena. Typically, these are characterized by metastable, supercooled states and the nucleation of bubbles. Applications range from the condensation of water vapor to the vacuum decay of fundamental quantum fields. In cosmology, bubbles of a new matter phase would produce huge density variations, and unsurprisingly first order phase transitions have been proposed as sources of gravitational waves [1,2] and as sources of primordial black holes [3,4].

Clearly a key factor in the relevance of such by-products of phase transitions is the likelihood of that transition occurring. Bubble nucleation rates are exponentially suppressed, and formal estimates of the lifetimes of metastable states can be huge. However, many phase transition rates in ordinary matter are greatly enhanced by the presence of nucleation seeds, in the form of impurities or defects on the boundary of the material. We have argued recently that cosmological bubble nucleation can also be greatly accelerated by nucleation seeds, for example with seeds in the form of primordial black holes [5,6]. In this paper we propose that seeded bubble nucleation can be studied in a laboratory cold-atom analogue of cosmological vacuum decay [7,8].

The idea of using analogue systems for cosmological processes comes under the general area of modeling the "universe in the laboratory" [9,10]. So far, analogue systems have mostly been employed to test ideas in perturbative quantum field theory [11,12], but nonperturbative phenomena such as bubble nucleation also play an important role in quantum mechanics and field theory.

As pointed out in the classic work of Coleman and others [13–15], the bubble nucleation process in quantum field theory can be described by an *instanton*, or *bounce*, solution to the field equations in imaginary time. The probability for decay is then given, to leading order, by a negative exponential of the action of the instanton. Understanding vacuum decay and the role of the instanton is now particularly pressing in light of the measurements of the Higgs mass, that currently indicates our vacuum is in a region of metastability [16].

The semiclassical description of vacuum decay with gravity involves analytically continuing to imaginary time, and finding the gravitational instanton. However, while most are comfortable with the assumptions used in perturbative quantum field theory on curved spacetime, such nonperturbative processes are sometimes viewed with more caution. The ability to test such a process via an analogue "table-top" quantum system would be a strong vindication of the use of such techniques. To this end, there have been some recent developments in exploring possible analogue systems that could test vacuum decay. Fialko *et al.* [7,8] proposed an experiment in a laboratory cold atom system. Their system consists of a Bose gas with two different spin states of the same atom species in an optical trap. The two

[*]thomas.billam@ncl.ac.uk
[†]r.a.w.gregory@durham.ac.uk
[‡]florent.c.michel@durham.ac.uk
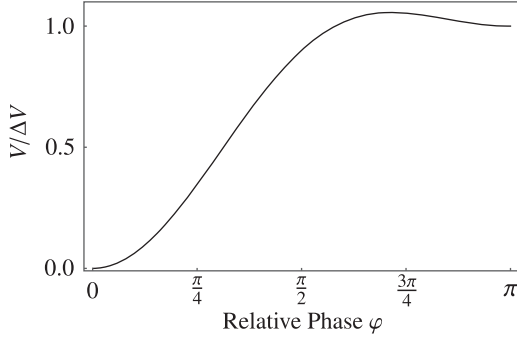[§]ian.moss@ncl.ac.uk

FIG. 1.   The field potential V plotted as a function of the relative phase of the two atomic wave functions, φ. The false vacuum is the minimum at $\varphi = \pi$ and the true vacuum the global minimum at $\varphi = 0$. ΔV is the difference in vacuum energy.

states are coupled by a microwave field. By modulating the amplitude of the microwave field, a new quartic interaction between the two states is induced in the time-averaged theory which creates a nontrivial ground state structure as illustrated in Fig. 1 [17].

In this paper we propose an analogue system that can explore the process of catalysis of vacuum decay that is central to our previous results. We use the above model to test seeded vacuum decay by introducing a vortex into the two dimensional spinor Bose gas system. We have used two complementary theoretical approaches. First, we have applied Coleman's non-perturbative theory of vacuum decay to the Gross-Pitaevskii equation (GPE). Second, we have used the truncated Wigner method, a stochastic approach, to study the vacuum decay. In both cases, we find that the introduction of the vortex seed enhances the probability of vacuum decay.

II. SYSTEM

Our system is a two-component BEC of atoms with mass m coupled by a modulated microwave field. The Hamiltonian operator in n dimensions is given by

$$\hat{H} = \int d^n x \left\{ \psi_i^\dagger \left[\frac{-\hbar^2 \nabla^2}{2m} \right] \psi_i + V(\psi_i, \psi_i^\dagger) \right\}, \quad (1)$$

with field operators ψ_i, $i = 1, 2$ and summation over the spin indices implied. Fialko et al. [7,8] described a procedure whereby averaging over timescales longer than the modulation timescale leads to an interaction potential of the form

$$V = \frac{g}{2} (\psi_i^\dagger)^2 (\psi_i)^2 - \mu \psi_i^\dagger \psi_i - \nu \psi_i^\dagger \sigma_{xij} \psi_j + \frac{g \nu \lambda^2}{4\mu} (\psi_i^\dagger \sigma_{yij} \psi_j)^2, \quad (2)$$

where the σ_i are the Pauli matrices. The potential includes the chemical potential μ, intracomponent s-wave

interactions of strength g between the field operators (we assume intercomponent s-wave interactions are negligible), and the microwave induced interaction ν. The final term comes from the averaging procedure and introduces a new parameter λ, dependent on the amplitude of the modulation. The trapping potential used to confine the condensate has been omitted in order to isolate the physics of vacuum decay.

The terms proportional to ν are responsible for the difference in energy between the global and local minima of the energy. The global minimum represents the true vacuum state and the local minimum represents the false vacuum. In order to parametrize the difference in energy between the vacua, we introduce a "small" dimensionless parameter ϵ by

$$\epsilon = \left(\frac{\nu}{\mu} \right)^{1/2}. \quad (3)$$

For $\nu > 0$, the true vacuum is a state with $\psi_1 = \psi_2$ and the false vacuum is a state with $\psi_1 = -\psi_2$. The condensate densities of the two components at the extrema are equal to one another, and given by $\langle \psi_1^\dagger \psi_1 \rangle = \langle \psi_2^\dagger \psi_2 \rangle = \rho_m (1 \pm \epsilon^2)$. Note that we prefer to work with the mean density $\rho_m = \mu/g$ rather than the chemical potential. The difference in energy density between the two vacuum states is given by $\Delta V = 4g \rho_m^2 \epsilon^2$.

III. INSTANTON TREATMENT

The nonperturbative theory of vacuum decay starts with the imaginary-time partition function

$$Z = \int D\psi_i D\bar{\psi}_i e^{-S[\psi_i, \bar{\psi}_i]/\hbar}, \quad (4)$$

where the integral extends over complex fields ψ_i and their complex conjugates $\bar{\psi}_i$ with action

$$S[\psi_i, \bar{\psi}_i] = \int d^n x d\tau \left\{ \hbar \bar{\psi}_i \partial_\tau \psi_i - \bar{\psi}_i \frac{\hbar^2}{2m} \nabla^2 \psi_i + V(\psi_i, \bar{\psi}_i) \right\}. \quad (5)$$

Vacuum decay is associated with instanton solutions to field equations in imaginary time $\tau = it$ [13,14]

$$\frac{\hbar^2}{2m} \nabla^2 \psi_i - \hbar \partial_\tau \psi_i - \frac{\partial V}{\partial \bar{\psi}_i} = 0,$$

$$\frac{\hbar^2}{2m} \nabla^2 \bar{\psi}_i + \hbar \partial_\tau \bar{\psi}_i - \frac{\partial V}{\partial \psi_i} = 0, \quad (6)$$

and fields that approach the false vacuum as $r, \tau \to \infty$.

On the original path integration contour, ψ_i and $\bar{\psi}_i$ are complex conjugates and the field equations imply that the saddle points are static. In order to find the nonstatic bubble

solutions, we have to deform the path of integration into a wider region of complex function space where $\bar\psi_i$ is not the complex conjugate of ψ_i. Although this may appear a strange procedure at first sight, this analytic continuation is already implicit in the previous work on vacuum decay as we shall see later.

The full expression for the nucleation rate of vacuum bubbles in a volume $\mathcal{V}$ is [13,14],

$$\Gamma \approx \mathcal{V} \left| \frac{\det' S''[\psi_b]}{\det S''[\psi_{\rm fv}]} \right|^{-1/2} \left(\frac{S[\psi_b]}{2\pi\hbar} \right)^{N/2} e^{-S[\psi_b]/\hbar}. \quad (7)$$

where S'' denotes the second functional derivative of the action S, and $\det'$ denotes omission of $N = n + 1$ zero modes from the functional determinant of the operator. (For convenience, we always include a constant shift to the action so that the action of the false vacuum is zero.) For seeded nucleation, the volume factor is replaced by the number of nucleation seeds and the number of zero modes becomes $N = 1$. The key feature here is the exponential suppression of the decay rate, and the nonperturbative treatment fails if the exponent is small.

In vacuum decay, the key quantity determining physical aspects of decay is the energy splitting between true and false vacua, ΔV, which is proportional to ϵ^2. In our system, ϵ also determines the magnitude of the interaction between the two scalars, and for small ϵ, most of the degrees of freedom of the system decouple, leaving an effective field theory of the relative phases of the two condensates as explored in [7,8] in one spatial dimension.

Here we are interested in seeded decay, so we consider the model in *two* spatial dimensions with polar coordinates r and θ. The natural size of the bubble will be determined by $R_0 = \hbar(\rho_m/m\Delta V)^{1/2}$, and the natural timescale by R_0/c_s, where the sound speed $c_s = (g\rho_m/m)^{1/2}$. To simplify the following analysis, we rescale our dimensionful coordinates accordingly, and also rescale the action:

$$S = \hbar\rho_m R_0^2 \hat{S}. \quad (8)$$

Since we are interested in exploring seeded decay, we look for a cylindrically symmetric solution that explicitly highlights the relevant degrees of freedom—namely, the relative phase $\varphi(r,\tau)$ between the two components, the leading order (in ϵ) profile of the false vacuum background $\rho(r,\tau)$, an overall common phase winding $n\theta$ that is present in a nontrivial vortex background, and the bubble profile function $\sigma(r,\tau)$—and includes the possibility of a topologically nontrivial vortex false vacuum state:

$$\psi_i = \rho^{1/2}\left(1 \pm \frac{\epsilon}{2}\sigma\right) e^{\pm i\varphi/2 + in\theta},$$

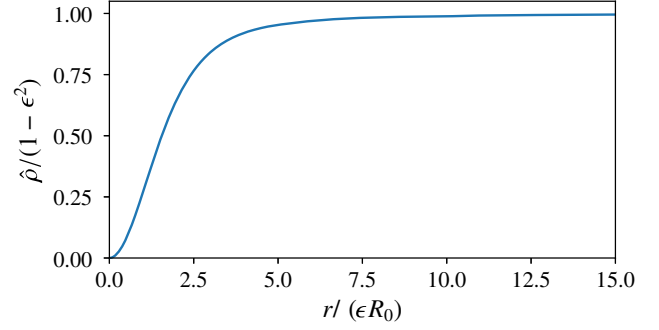$$\bar\psi_i = \rho^{1/2}\left(1 \pm \frac{\epsilon}{2}\sigma\right) e^{\mp i\varphi/2 - in\theta}, \quad (9)$$

FIG. 2. Vortex density profile $\hat\rho = \rho/\rho_m$ plotted as a function of radius r. The density vanishes at the center and approaches the false vacuum density as $r \to \infty$. Its physical thickness scales as ϵR_0.

where we adopt the convention that the upper/lower signs apply to the $i = 1, 2$ spin states respectively.

The pure false vacuum has $n = 0$, and $\rho = \rho_m(1 - \epsilon^2)$, with instanton profiles for φ explored in [7,8]. Here we are interested in seeded tunneling, so we also consider the vortex background for $n = 1$, with ρ satisfying the $\mathcal{O}(\epsilon^2)$ background equations obtained by substituting (9) in (6). The profile of ρ is precisely that of a superfluid (or global) vortex, and is illustrated in Fig. 2.

The potential for the instanton solutions depends only on the relative phase φ and the background density ρ. Our rescaling of the length and time coordinates means that we also rescale the potential to $\hat{V} = 2(V - V_{TV})/\Delta V$,

$$\hat{V} = \hat\rho(1 - \cos\varphi) + \frac{1}{2}\lambda^2\hat\rho^2\sin^2\varphi, \quad (10)$$

as plotted in Fig. 1. At zeroth order in ϵ, the field equations (6) imply that $\sigma = -i\hat\rho^{-1}\partial_\tau\varphi$. Note that σ is imaginary, and the bubble solution has $\bar\psi_1 \neq \psi_1^\dagger$ as was mentioned earlier. Replacing σ in the action using this field equation gives a Klein-Gordon type action depending only on φ which was used in Refs. [7,8]:

$$\hat{S}[\varphi] = \epsilon \int d^n x d\tau \left\{ \frac{1}{2}\hat\rho(\nabla\varphi)^2 + \frac{1}{2}\dot\varphi^2 + \hat{V} \right\}. \quad (11)$$

However, at the core of the vortex, $\hat\rho \to 0$ and this replacement of σ is no longer valid. Instead, numerical solutions have been obtained by solving the full equations for the phase φ and the density variation σ.

The vacuum decay rate around a single vortex, using Coleman's formula (7) with a single zero mode, is

$$\Gamma = A\frac{c_s}{R_0}\left(\frac{\rho_m R_0^2 \hat{S}}{2\pi}\right)^{1/2} e^{-\rho_m R_0^2 \hat{S}}, \quad (12)$$

where A is a dimensionless numerical factor depending on the ratio of determinants (which we do not evaluate here).
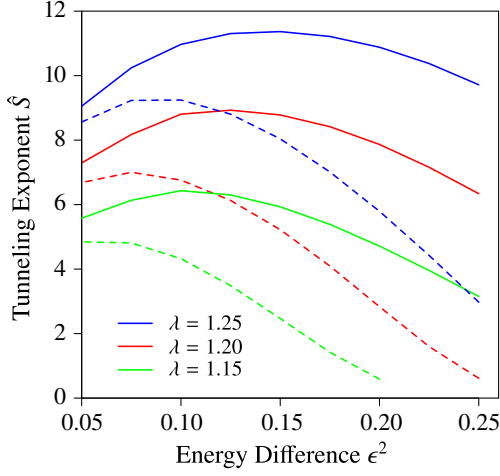
FIG. 3. The dimensionless exponent $\hat{S}$ of the vacuum decay rate plotted as a function of the parameter ϵ^2. The solid lines represent unseeded vacuum decay and the dashed lines are for bubbles seeded by vortices. The action is lower for the seeded bubbles.

Numerical results for the factor $\hat{S}$ in the decay exponent are shown in Fig 3 [20]. These show clearly that the tunneling exponent can be reduced significantly in the presence of a vortex. The vortex width from Fig. 2 is related to ϵR_0. Consequently, smaller values of ϵ are associated with relatively thin vortices compared to the bubble scale R_0, which have less effect on the vacuum decay rate than vortices with larger values of ϵ.

The nucleation rate depends on the physical parameters through the combination $\rho_m R_0^2$. The length scale R_0 itself is related to the atomic scattering length a_s and the thickness of the condensate a_z via the effective coupling strength g, [22],

$$g = \frac{4\pi\hbar^2}{m}\frac{a_s}{\sqrt{2\pi}a_z}. \tag{13}$$

Thus the factor in the decay exponent becomes $\rho_m R_0^2 = a_z/(4\epsilon^2\sqrt{8\pi}a_s)$.

IV. STOCHASTIC TREATMENT

A. Overview

As an alternative treatment of bubble nucleation we model a two-dimensional spinor BEC using a truncated Wigner approach. At the mean-field level, the system can be described by the Gross-Pitaevskii equation (GPE) derived from the symmetric Hamiltonian in the rescaled coordinates used above,

$$i\partial_t\psi_i = -\epsilon\nabla^2\psi_i + \epsilon\hat{V}_T\psi_i + \epsilon\rho_m\frac{\partial\hat{V}}{\partial\bar{\psi}_i}, \tag{14}$$

where

$$\frac{\partial\hat{V}}{\partial\bar{\psi}_i} = \frac{1}{2\epsilon^2}\left(\frac{\bar{\psi}_i\psi_i}{\rho_m} - 1\right)\frac{\psi_i}{\rho_m} - \frac{1}{2}\frac{(\sigma_x\psi)_i}{\rho_m} + \frac{\lambda^2}{4}\frac{\bar{\psi}\sigma_y\psi}{\rho_m}\frac{(\sigma_y\psi)_i}{\rho_m}. \tag{15}$$

Here $\hat{V}_T$ is the dimensionless form of an optical trapping potential that affects both spin states equally. The dimensional trapping potential is $V_T = 2g\rho_m\epsilon^2\hat{V}_T$. The truncated Wigner approach seeks to emulate the many-body quantum field description of a BEC with a stochastic description [23,24]. At zero temperature, it consists of seeding appropriate modes of the system with an average of $1/2$ particle per mode of stochastic noise in the initial conditions, and then evolving in time with the GPE. The stochastic noise emulates vacuum fluctuations.

We add stochastic noise to an ensemble of initial fields and compute the trajectory of each field using the projected GPE (PGPE) to precisely evolve the noise-seeded modes [24], including a correction to the nonlinear term to account for the average noise density [8]. In a periodic 2D square box of side length L this corresponds to propagating the equation

$$i\partial_t\psi_i = \mathcal{P}\left\{\left[-\epsilon\nabla^2 + \epsilon\hat{V}_T + \frac{|\psi_i|^2 - \frac{M}{L^2}}{2\epsilon\rho_m} - \frac{1}{2\epsilon}\right]\psi_i + \left[-\frac{\epsilon}{2} + \frac{\epsilon\lambda^2}{4\rho_m}(\psi_i\psi_{3-i}^* - \psi_i^*\psi_{3-i})\right]\psi_{3-i}\right\}, \tag{16}$$

where the projection operator $\mathcal{P}$ restricts the field to the M lowest-energy plane wave modes.

B. Vortex-seeded decay in an infinite system

Taking a periodic 2D square box of side length L, we begin with the false vacuum solution to the GPE,

$$\psi_{iFV} = \rho_m^{1/2}(1 - \epsilon^2)^{1/2}e^{\pm i\pi/2}. \tag{17}$$

We evolve the PGPE (16) using a Fourier pseudospectral method, implemented using XMDS2 software [25], with P grid points in each direction. The projector $\mathcal{P}$ restricts the field to the M modes satisfying $|\mathbf{k}| < \pi P/(2L)$. Thus, we create an initial ensemble of fields by adding noise into these M plane-wave modes:

$$\psi_i = \psi_{iFV} + \frac{1}{L}\mathcal{P}\left\{\sum_{\mathbf{k}}\beta_{i\mathbf{k}}e^{i\mathbf{k}\cdot\mathbf{r}}\right\}, \tag{18}$$

where $\beta_{i,\mathbf{k}}$ are complex Gaussian random variables with $\langle\beta_{i,\mathbf{k}}^*\beta_{j,\mathbf{k}'}\rangle = \delta_{i,j}\delta_{\mathbf{k},\mathbf{k}'}/2$. To determine a decay rate without vortices, we evolve trajectories directly from this initial ensemble.

To investigate the effects of vortices on the decay rate we take an initial ensemble as described above, but prior to evolving trajectories we imprint the density and phase profiles of vortices into the system. Since our periodic box

requires a net-neutral distribution of vortices, we use the techniques described in Ref. [26] to imprint a square grid pattern comprising two clockwise-circulating and two anticlockwise-circulating vortices. The vortices' mutual x and y separations are set to $L/2$, and diagonally opposed vortices have the same circulation.

In Fig. 4 we show typical examples of the stochastic trajectories with and without the imprinted vortices. [These are frames from the movies included as Supplemental Material [27].] We observe bubbles of true vacuum to nucleate most often at the locations of the vortices when they are present, although nucleation in the bulk does remain possible in the presence of vortices. To quantitatively investigate the increase in the rate of nucleation we evolve an ensemble of 1000 trajectories both with and without vortices. As in Ref. [8], we evaluate the average value of $\cos\phi$ across all simulation grid points in each trajectory, and consider a trajectory to have nucleated a

FIG. 5. Fraction of trajectories failing to nucleate a bubble of true vacuum by a given time, $F(t)$, both with and without vortices (dashed and solid lines respectively). The straight grey lines show exponential decays, fitted over selected regions.

bubble of true vacuum when this average exceeds -0.95. In Fig. 5 we plot the fraction of trajectories that have failed to nucleate a bubble as a function of time, $F(t)$. We determine approximate decay rates by least-squares fitting an exponential decay to $F(t)$ over the time interval where it best resembles an exponential decay (determined by eye from Fig. 5). Taking $\lambda = 1.15$, we find $\Gamma \approx (2.9 \pm 0.1) \times 10^{-3} c_s/R_0$ without vortices, and $\Gamma \approx (26 \pm 2) \times 10^{-3} c_s/R_0$ with vortices. For $\lambda = 1.2$, we find $\Gamma \approx (1.9 \pm 0.2) \times 10^{-5} c_s/R_0$ without vortices, and $\Gamma \approx (700 \pm 20) \times 10^{-5} c_s/R_0$ with vortices. The quoted uncertainties estimate the statistical uncertainty in the stochastic method by a bootstrap calculation [28]. Clearly, the presence of vortices greatly enhances the rate of vacuum decay in this system.

C. Vortex-seeded decay in a trapped system

To investigate the potential for realizing these results in experiments, we repeat our stochastic simulations for the case of a spinor BEC contained inside a circular optical "bucket" trap of radius R

$$\hat{V}_T(r) = \frac{\hat{V}_0}{2}\left[1 + \tanh\left(\frac{r-R}{w}\right)\right], \qquad (19)$$

where $\hat{V}_0$ is the (dimensionless) trap depth and w parametrizes the wall-steepness of the trap. We apply the truncated Wigner formalism as described above, but making an approximation for the initial stochastic noise,

$$\psi_i = \psi_{iFV} + \frac{f(r)}{L}\mathcal{P}\left\{\sum_{\mathbf{k}} \beta_{i\mathbf{k}}e^{i\mathbf{k}\cdot\mathbf{r}}\right\} \qquad (20)$$
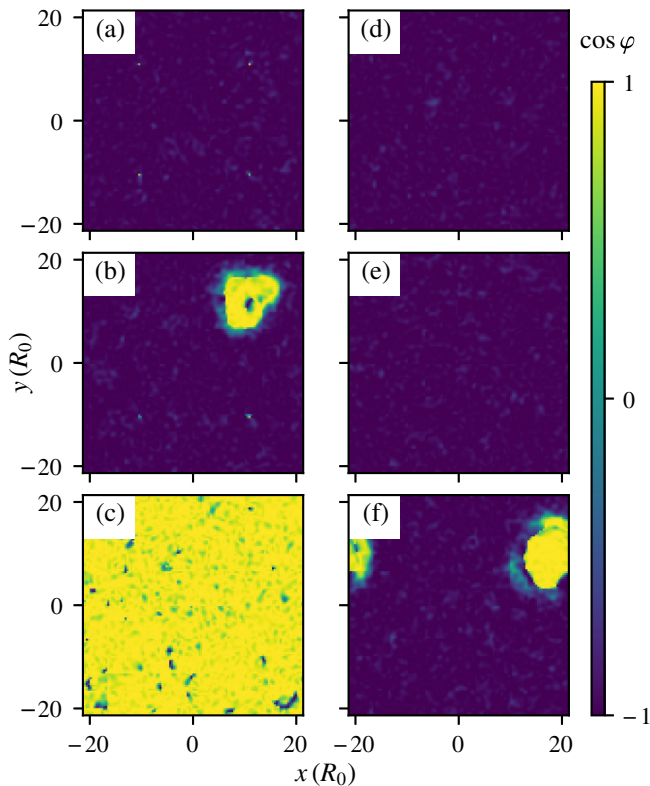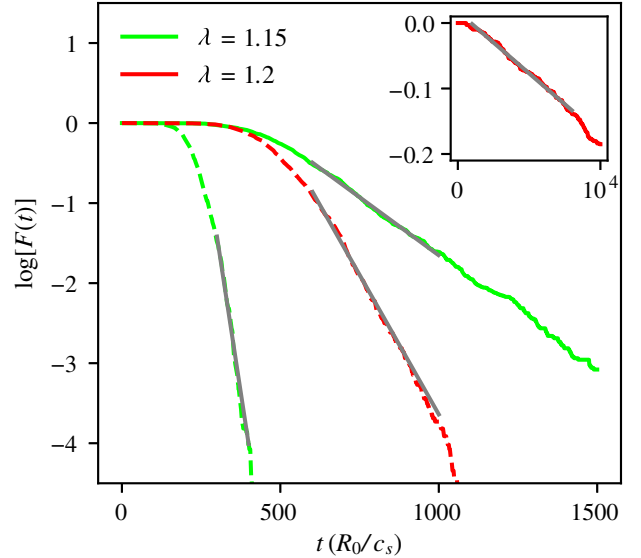

FIG. 4. Typical examples of the decay of the false vacuum with and without imprinted vortices in a two-dimensional periodic system. The plots show the cosine of the relative phase between the two spin states. Dimensionless parameters are $\lambda = 1.15$, $\epsilon = 0.316$, $\rho_m R_0^2 = 60.0$, and $L = 42.67R_0$. Our numerical grid has $P = 128$. (a) Initially, the false vacuum predominates. (b) As time progresses, bubbles of true vacuum (yellow) nucleate, predominantly around the vortices. (c) Later still, nucleated bubbles expand to fill the system. (d–f) Typical trajectories without imprinted vortices [same times as (a–c)] illustrate the nucleation of bubbles at random locations, which occurs at a slower rate than vortex-seeded nucleation.

where the function $f(r) = \Theta(R - r)$ restricts the noise to the trap interior. We then evolve the PGPE as described above, both with and without initial imprinting of the density and phase profiles of a vortex at the trap center.

Numerical results, shown in Fig. 6, confirm that the vortex continues to act as nucleation seed in this system, holding out the possibility of experimental observation of this effect. However, we also observe that the walls of the trap strongly enhance bubble nucleation, both with and without the imprinted vortex. Our numerics show that the rate of vortex seeding at the trap walls is dependent on the wall steepness w, with steeper walls reducing the rate. This is a boundary effect, due to the fact that the density outside of the trap is low, allowing the phase to fluctuate widely, as seen in the first frame of Fig. 6. This could be interpreted as the exterior of the trap being full of "ghost"
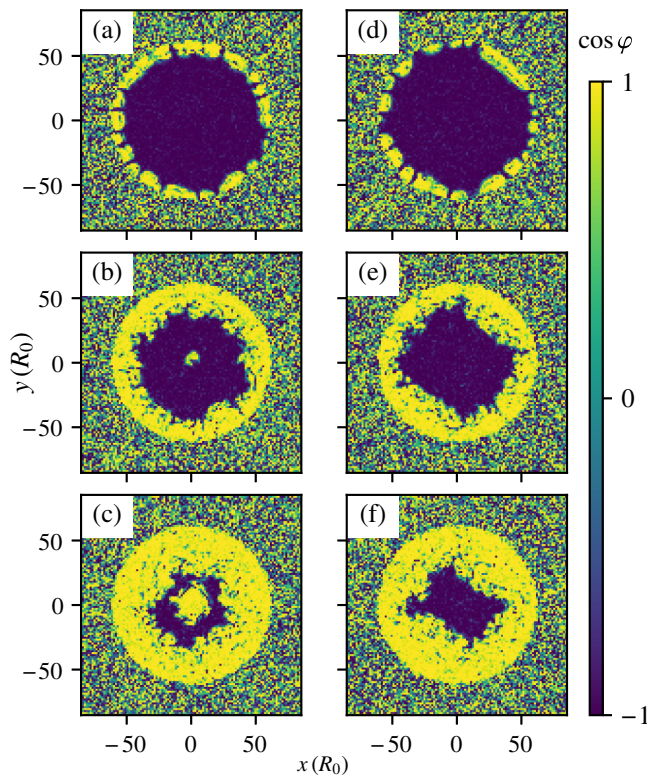
vortices that then migrate to the wall and trigger bubble nucleation, and may be of interest for laboratory BECs. However, in an unbounded system such as our universe, this boundary effect is irrelevant, and the only possible seed will be the vortex.

V. CONCLUSION

In conclusion, our two theoretical approaches, based on the Euclidean field equations (6) and on the truncated Wigner approximation, both show a significant increase of the decay rate of the false vacuum in the presence of a vortex, in agreement with our previous work on cosmological phase transitions. Both the quantum calculation and the TW approach agree on this conclusion, although the TW approach gives faster vacuum decay in all cases than the quantum calculation does. We believe this is likely to be due to the energy content of the stochastic fluctuations which gives a boost to crossing the potential barrier. It may be possible to account for this effect by renormalizing the parameters of the potential in the TW approach. We plan to investigate this further, and conduct a thorough comparison of the different approaches in a simpler 1D system.

Numerical simulations also indicate that other kinds of defects, such as the walls of a sharp potential trap, can also enhance decay. Since getting a large enough decay rate is a major difficulty in designing experiments, we expect this to be an important ingredient for putting the theoretical model of [7,8] into practice, and thus testing vacuum decay in the laboratory. While our simulations represent a proof-of-principle example rather than a concrete experimental proposal, advances in optical trapping [29,30] and various techniques for vortex imprinting in spinor condensates [31,32] could be used to probe similar systems experimentally.

Data supporting this publication is openly available under a Creative Commons CC-BY-4.0 License [33].

FIG. 6. Examples of the decay of the false vacuum with and without an imprinted vortex in a two-dimensional "bucket" trap. The plots show the cosine of the relative phase between the two spin states. Dimensionless parameters are $\lambda = 1.15$, $\epsilon = 0.316$, $\rho_m R_0^2 = 32.0$, and $L = 170.68 R_0$. Our numerical grid has $P = 512$. The BEC is contained inside a circular bucket trap, $\hat{V}_T(r) = \hat{V}_0 \{1 + \tanh[(r - R)/w]\}/2$, parametrized by strength $\hat{V}_0 = 100$, radius $R = 64 R_0$ and wall steepness $w = 2 R_0$. (a) Initially, the false vacuum predominates within the circular trap, but bubbles of true vacuum rapidly form around the walls of the trap. (b) Later, a bubble of true vacuum (yellow) forms around the vortex in the center. (c) Later still, the true vacuum regions grow, and eventually merge. (d–f) Typical trajectory without an initially imprinted vortex [same times as (a–c)].

[1] C. Caprini, R. Durrer, T. Konstandin, and G. Servant, Phys. Rev. D **79**, 083519 (2009).

[2] M. Hindmarsh, S. J. Huber, K. Rummukainen, and D. J. Weir, Phys. Rev. Lett. **112**, 041301 (2014).

[3] S. W. Hawking, I. G. Moss, and J. M. Stewart, Phys. Rev. D **26**, 2681 (1982).

[4] H. Deng and A. Vilenkin, J. Cosmol. Astropart. Phys. 12 (2017) 044.

[5] R. Gregory, I. Moss, and B. Withers, J. High Energy Phys. 03 (2014) 081.

[6] P. Burda, R. Gregory, and I. Moss, Phys. Rev. Lett. **115**, 071303 (2015).

[7] O. Fialko, B. Opanchuk, A. I. Sidorov, P. D. Drummond, and J. Brand, Europhys. Lett. **110**, 56001 (2015).

[8] O. Fialko, B. Opanchuk, A. I. Sidorov, P. D. Drummond, and J. Brand, J. Phys. B At. Mol. Opt. Phys. **50**, 024003 (2017).

[9] T. Roger, C. Maitland, K. Wilson, N. Westerberg, D. Vocke, E. M. Wright, and D. Faccio, Nat. Commun. **7**, 13492 (2016).

[10] S. Eckel, A. Kumar, T. Jacobson, I. B. Spielman, and G. K. Campbell, Phys. Rev. X **8**, 021021 (2018).

[11] W. G. Unruh, Phys. Rev. Lett. **46**, 1351 (1981).

[12] C. Barcelo, S. Liberati, and M. Visser, Living Rev. Relativity **8**, 12 (2005); **14**, 3 (2011).

[13] S. R. Coleman, Phys. Rev. D **15**, 2929 (1977); **16**, 1248(E) (1977).

[14] C. G. Callan and S. R. Coleman, Phys. Rev. D **16**, 1762 (1977).

[15] S. R. Coleman and F. De Luccia, Phys. Rev. D **21**, 3305 (1980).

[16] G. Degrassi, S. Di Vita, J. Elias-Miro, J. R. Espinosa, G. F. Giudice, G. Isidori, and A. Strumia, J. High Energy Phys. 08 (2012) 098.

[17] It has been pointed out that there is an instability in the equations describing the modulated system [18,19]. However, for the parameters used in this paper and trap radius 25 μm with ^{39}K, the instability occurs for a modulation frequency $\omega < 800k^2$ Hz, where k is the maximum wave number consistent with the equations, in units of the healing length. We will assume that the modulation frequency is above this limit.

[18] J. Braden, M. C. Johnson, H. V. Peiris, A. Pontzen, and S. Weinfurtner, Phys. Rev. Lett. **123**, 031601 (2019).

[19] J. Braden, M. C. Johnson, H. V. Peiris, and S. Weinfurtner, J. High Energy Phys. 07 (2018) 014.

[20] We have checked these results using an ansatz approach akin to that of [21], extended to include dispersion. The results agree within a few per cent.

[21] B.-H. Lee, W. Lee, R. MacKenzie, M. B. Paranjape, U. A. Yajnik, and D.-h. Yeom, Phys. Rev. D **88**, 085031 (2013).

[22] M. D. Lee, S. A. Morgan, M. J. Davis, and K. Burnett, Phys. Rev. A **65**, 043617 (2002).

[23] S. Chaturvedi and P. D. Drummond, Eur. Phys. J. B **8**, 251 (1999).

[24] P. Blakie, A. Bradley, M. Davis, R. Ballagh, and C. Gardiner, Adv. Phys. **57**, 363 (2008).

[25] G. R. Dennis, J. J. Hope, and M. T. Johnsson, Comput. Phys. Commun. **184**, 201 (2013).

[26] T. P. Billam, M. T. Reeves, B. P. Anderson, and A. S. Bradley, Phys. Rev. Lett. **112**, 145301 (2014).

[27] See Supplemental Material at http://link.aps.org/supplemental/10.1103/PhysRevD.100.065016 for movies showing examples of the dynamics.

[28] We estimate the uncertainties in the rate by a two-step bootstrap procedure: First we create 250 sample datasets (of 1000 trajectories each) by randomly choosing trajectories from our actual dataset of 1000 trajectories with replacement. Secondly we fit an exponential decay to each sample dataset using least-squares fitting as described above. The quoted error is the standard deviation of the distribution of 250 rates obtained from fitting these sample datasets. The uncertainty obtained by this simple estimate is orders of magnitude larger that the least-squares fitting error of a single dataset, suggesting the latter is not a realistic estimate of the overall uncertainty.

[29] A. L. Gaunt, T. F. Schmidutz, I. Gotlibovych, R. P. Smith, and Z. Hadzibabic, Phys. Rev. Lett. **110**, 200406 (2013).

[30] G. Gauthier, I. Lenton, N. M. Parry, M. Baker, M. J. Davis, H. Rubinsztein-Dunlop, and T. W. Neely, Optica **3**, 1136 (2016).

[31] Y. Kawaguchi and M. Ueda, Phys. Rep. **520**, 253 (2012).

[32] D. M. Stamper-Kurn and M. Ueda, Rev. Mod. Phys. **85**, 1191 (2013).

[33] T. P. Billam, R. Gregory, F. Michel, and I. G. Moss, Data supporting publication: Simulating seeded vacuum decay in a cold atom system, https://.doi.org/10.25405/data.ncl.9639143.